Article

Cell Reports

Insertional Mutagenesis Identifies a STAT3/Arid1b/β-catenin Pathway Driving Neurofibroma Initiation

Graphical Abstract

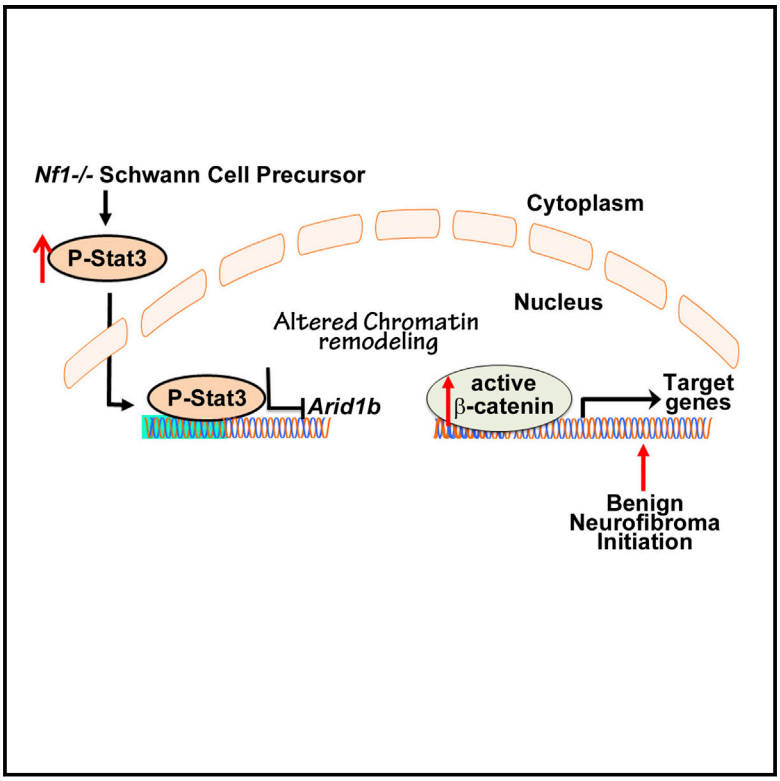

Authors

Jianqiang Wu, Vincent W. Keng, Deanna M. Patmore, ..., Robert J. Spinner, David A. Largaespada, Nancy Ratner

Correspondence

nancy.ratner@cchmc.org

In Brief

Wu et al. map an *Nf1-Stat3-Arid1b/β-catenin* pathway that initiates Neurofibromatosis type 1 (*Nf1*) neurofibromas, using unbiased insertional mutagenesis screening. *Stat3* transcriptionally represses *Gsk3β* and *Arid1b*, thereby activating β-catenin in Schwann cell precursors and resulting in neurofibroma initiation and maintenance. Stat3-mediated modification plays a role in early tumorigenesis.

Highlights

- Insertional mutagenesis identifies *STAT3* as a driver of benign neurofibromas
- Stat3 activates β-catenin to initiate neurofibroma formation
- Stat3 represses *Gsk3β* and *Arid1b* to increase β-catenin
- Neurofibroma-initiating cells require Stat3 and β-catenin for tumorigenesis

Wu et al., 2016, Cell Reports *14*, 1979–1990
March 1, 2016
http://dx.doi.org/10.1016/j.celrep.2016.01.074

Cell Reports
Article

Insertional Mutagenesis Identifies a STAT3/Arid1b/β-catenin Pathway Driving Neurofibroma Initiation

Jianqiang Wu,[1] Vincent W. Keng,[3,4,5,13] Deanna M. Patmore,[1] Jed J. Kendall,[1] Ami V. Patel,[1] Edwin Jousma,[1] Walter J. Jessen,[1] Kwangmin Choi,[1] Barbara R. Tschida,[3,5] Kevin A.T. Silverstein,[6] Danhua Fan,[6] Eric B. Schwartz,[7] James R. Fuchs,[7] Yuanshu Zou,[2] Mi-Ok Kim,[2] Eva Dombi,[8] David E. Levy,[9] Gang Huang,[1] Jose A. Cancelas,[1,10] Anat O. Stemmer-Rachamimov,[11] Robert J. Spinner,[12] David A. Largaespada,[3,4,5] and Nancy Ratner[1,*]

[1]Division of Experimental Hematology and Cancer Biology, Cancer and Blood Diseases Institute, Cincinnati Children's Hospital University of Cincinnati, Cincinnati, OH 45229, USA
[2]Division of Biostatistics and Epidemiology, Cincinnati Children's Hospital Research Foundation, Cincinnati Children's Hospital University of Cincinnati, Cincinnati, OH 45229, USA
[3]Masonic Cancer Center, University of Minnesota, Minneapolis, MN 55455, USA
[4]Department of Pediatrics, Cell Biology and Development, University of Minnesota, Minneapolis, MN 55455, USA
[5]Center for Genome Engineering, University of Minnesota, Minneapolis, MN 55455, USA
[6]Biostatistics and Informatics, University of Minnesota, Minneapolis, MN 55455, USA
[7]Ohio State University, College of Pharmacy, Columbus, OH 43210, USA
[8]Pediatric Oncology Branch, National Cancer Institute, Bethesda, MD 20892, USA
[9]Department of Pathology and New York University Cancer Institute, New York University School of Medicine, 550 First Avenue, New York, NY 10016, USA
[10]Hoxworth Blood Center, College of Medicine, University of Cincinnati, Cincinnati, OH 45267, USA
[11]Department of Pathology, Massachusetts General Hospital and Harvard Medical School, Boston, MA, 02114, USA
[12]Department of Neurologic Surgery, Mayo Clinic, Rochester, MN 55905, USA
[13]Present address: Department of Applied Biology and Chemical Technology, the Hong Kong Polytechnic University, Hung Hom, Kowloon, Hong Kong
*Correspondence: nancy.ratner@cchmc.org
http://dx.doi.org/10.1016/j.celrep.2016.01.074

SUMMARY

To identify genes and signaling pathways that initiate Neurofibromatosis type 1 (NF1) neurofibromas, we used unbiased insertional mutagenesis screening, mouse models, and molecular analyses. We mapped an *Nf1-Stat3-Arid1b/β-catenin* pathway that becomes active in the context of *Nf1* loss. Genetic deletion of *Stat3* in Schwann cell progenitors (SCPs) and Schwann cells (SCs) prevents neurofibroma formation, decreasing SCP self-renewal and β-catenin activity. β-catenin expression rescues effects of Stat3 loss in SCPs. Importantly, P-STAT3 and β-catenin expression correlate in human neurofibromas. Mechanistically, P-Stat3 represses *Gsk3β* and the SWI/SNF gene *Arid1b* to increase β-catenin. Knockdown of *Arid1b* or *Gsk3β* in *Stat3*$^{fl/fl}$;*Nf1*$^{fl/fl}$;*DhhCre* SCPs rescues neurofibroma formation after in vivo transplantation. Stat3 represses *Arid1b* through histone modification in a *Brg1*-dependent manner, indicating that epigenetic modification plays a role in early tumorigenesis. Our data map a neural tumorigenesis pathway and support testing JAK/STAT and Wnt/β-catenin pathway inhibitors in neurofibroma therapeutic trials.

INTRODUCTION

Neurofibromas are benign peripheral nerve tumors that cause significant morbidity by disfigurement and tissue compression, and mortality if they compress vital organs (Boyd et al., 2009). Neurofibromas are a major feature of Neurofibromatosis type 1 (*NF1*), a common autosomal dominant disorder affecting about 1 in 3,500 individuals. Surgery remains the mainstay of neurofibroma therapy but is rarely curative, so new treatments are urgently needed.

Peripheral nerve Schwann cells (SCs) are the primary pathogenic cell in neurofibromas, as biallelic mutation or loss of *NF1* occurs uniquely in neurofibroma SCs (Serra et al., 1997). Neurofibromas may develop from SCs or Schwann cell progenitors (SCPs), because inactivation of *Nf1* at the SCP stage or in adult mice results in neurofibroma formation (Chen et al., 2014; Wu et al., 2008; Zhu et al., 2002). *NF1* encodes the RasGAP protein neurofibromin, and Ras signaling is elevated in neurofibroma SCs (Cichowski and Jacks, 2001). Other genes and signaling pathways that drive neurofibroma initiation and growth are largely unknown.

STAT3 is a latent transcription factor implicated in cancer, which regulates cell-cycle progression and apoptosis. STAT3 phosphorylation at Y705 is essential for STAT3 dimerization, required for STAT3 binding to DNA promoter regions and transcriptional activation (Battle and Frank, 2002). Fewer benign lesions formed when Stat3 was absent in prostate and skin tumors in vivo, implicating it in tumor initiation (Kim et al., 2009; Kroon et al., 2013). Stat3 also regulates self-renewal and growth of glioma stem cells (Sherry et al., 2009). Recent studies on malignant peripheral nerve sheath tumors (MPNSTs), aggressive nerve sarcomas, implicate Stat3 in their growth (Banerjee et al., 2010; Wu et al., 2014). The role of Stat3 in the benign nerve tumors (neurofibromas) has not been studied.

Stat3 activated β-catenin through GSK3b in hepatocytes (Moh et al., 2008). β-catenin is a developmental signaling pathway reactivated in many cancers. How β-catenin becomes elevated and if β-catenin plays a role in neurofibroma is unknown, although neurofibroma β-catenin expression was reported (Luscan et al., 2014; Mo et al., 2013; Watson et al., 2013). In vivo activation of β-catenin in developing SCs delays SC differentiation and results in sustained proliferation (Grigoryan et al., 2013), supporting possible roles for β-catenin in nerve tumorigenesis.

Multi-subunit SWI/SNF chromatin remodeling complexes modulate transcription factor access to target genes, resulting in activation or repression of transcription (Tolstorukov et al., 2013). Recent studies demonstrate mutation or loss of chromatin remodeling genes in progression to MPNSTs (De Raedt et al., 2014; Lee et al., 2014), but are unstudied in neurofibromas. Mutational inactivation of SWI/SNF complex genes, including *BRG1/SMARCA4*, encoding a SWI/SNF ATPase, and SWI/SNF subunit genes *ARID1A* and *ARID1B*, are increasingly implicated in development and cancer (Helming et al., 2014; Sausen et al., 2013). When an ARID1B-containing SWI/SNF complex is present, interaction of STAT3 with DNA activates *c-Myc* transcription in pre-osteoblast MC3T3-E1 cells (Nagl et al., 2007). Also, BRG1 interacts with β-catenin to promote target gene activation in colon cancer cells (Barker et al., 2001). In patients with intellectual disability, ARID1B represses *BRG1*-dependent Wnt/β-catenin signaling (Vasileiou et al., 2015).

We report results of an unbiased in vivo Sleeping Beauty insertional mutagenesis transposon screen. We demonstrate a critical role of Stat3 in driving neurofibromas. *Stat3* transcriptionally represses *Gsk3β* and the SWI/SNF complex subunit *Arid1b*, thereby activating β-catenin in SCPs and resulting in neurofibroma initiation and maintenance.

RESULTS

A Transposon System and Pathway Analysis Implicate the *Wnt* and *Stat3* Pathways in Neurofibroma Formation

To identify mechanisms underlying neurofibroma growth and/or tumor progression, we used insertional mutagenesis. We generated quadruple transgenic animals (*Nf1*$^{fl/fl}$*;DhhCre*;*Rosa26*-lsl-SB11;T2/Onc) (Figure S1A). Survival and onset of tumorigenesis did not differ from control animals (data not shown), and neurofibroma size was similar ($p = 0.1996$) (Figure S1B, top). However, the number of neurofibromas isolated from experimental animals was higher (5.4 versus 2.8; $p = 0.1017$) (Figure S1B, bottom). The trend toward significance in this small sample set suggests that transposition-related genes might play a role in increasing neurofibroma numbers and/or growth.

To identify potential genes responsible for neurofibroma tumorigenesis, we used high-throughput pyrosequencing of neurofibromas isolated from experimental quadruple transgenic animals. We identified 31 common transposon insertion sites (CISs). We removed CISs identified in control insertion-site mapping experiments in 3-week-old transgenic mouse tail DNA carrying both the T2/Onc and *Rosa26*-SB11 transgenes, and CISs identified in tumors from single mice. The remaining 22 CISs identified for neurofibroma tumorigenesis are shown in Figure 1A.

We used the Genemania prediction server (http://www.genemania.org) to predict pathways, interactions, and functions of the 22 CIS genes, and we identified networks including CIS genes. The most significantly deregulated pathways were *Wnt* signaling (false discovery rate [FDR] = 0.021) including CIS genes *Tnks* and *Gsk3β*, and major neighboring genes *Strn*, *Axin1*, and *Dvl1*, and *Stat3*-associated cellular carbohydrate metabolic process (FDR = 0.023) including the CIS genes *Gsk3β* and *Arid1b* and major neighboring genes *Stat3* and *Ptpn2* (Figure 1B). Interestingly, *Gsk3β* connected these two pathways in this in silico analysis. No tumor tissue from these mice was available for confirmatory analysis. The other signaling pathways identified by Genemania are shown in Figure S1C.

STAT3/β-catenin Signaling Is Activated in Mouse and Human Neurofibromas

We focused on STAT3, a known oncogene and therapeutic target unstudied in neurofibromas. Antibodies recognizing P-Stat3-Y705 detected positive cells in all genetically engineered mouse (GEM) neurofibromas (n = 19) (Figure 2A), but not wild-type (WT) mouse sciatic nerves (Figure 2A, inset). In contrast, P-Stat3-Ser727 was detectable in one out of four mice and one out of five human neurofibromas (data not shown). Given the link between the Stat and Wnt pathways identified by transposon mutagenesis, we tested if β-catenin is co-activated with P-Stat3 in neurofibroma SCs. *DhhCre* activates EGFP expression in the context of *DhhCreNf1*$^{fl/fl}$ mice in 40%–50% of SCs, in a reporter mouse in which the *CMV-β actin* promoter and *loxP* flanked CAT gene are upstream of the Egfp cassette (Nakamura et al., 2006). We stained frozen sections of *Nf1*$^{fl/fl}$*;DhhCre;EGFP* mouse neurofibromas with anti-P-Stat3 and anti-β-catenin. Of EGFP-expressing SCs, 21% were P-Stat3$^+$ only, 62% expressed only β-catenin$^+$, and, importantly, 6.7% of EGFP$^+$ SCs were P-Stat3$^+$ and β-catenin$^+$ (Figure 2B). Thus, P-Stat3 and β-catenin can be co-activated in SCs in neurofibromas. We also detected Iba1$^+$ macrophages that are P-Stat3$^+$;EGFP$^-$ (data not shown). Western blots confirmed robust P-Stat3-Y705 in mouse neurofibroma lysates versus WT peripheral nerve (Figure 2C).

We immunolabeled human plexiform neurofibroma sections to test if P-STAT3 and β-catenin expression correlate. Most (29/30) contained P-Y705-STAT3$^+$ and β-catenin$^+$ cells (Figures 2D–2F). Some neurofibroma cells showed cytoplasmic staining (43%), others showed nuclear staining (23%), and 34.2% showed

A

Gene	Chromosome	Neurofibromas, # with insertion (%)	Mice, # with insertion	Total # insertions	Predicted effect
Gsk3b	16	7 (14.3)	3	7	disrupt
Arid1b	17	5 (10.2)	4	7	disrupt
Slc35f1	10	6 (12.2)	5	6	unknown
Zfand3	17	5 (10.2)	4	6	disrupt
Tnks2	19	5 (10.2)	4	6	disrupt
Sorcs1	19	5 (10.2)	4	6	drive-C-term-truncate
Bre	5	5 (10.2)	3	6	disrupt
Zfp60	7	4 (8.2)	4	6	disrupt
Nefl	14	5 (10.2)	4	5	unknown
Chd2	7	5 (10.2)	4	5	disrupt
Picalm	7	5 (10.2)	2	5	disrupt
Prex2	1	4 (8.2)	3	4	drive-C-term-truncate
Gpbp1	13	4 (8.2)	4	4	disrupt
Wapal	14	4 (8.2)	3	4	drive-C-term-truncate
Gpc6	14	3 (6.1)	2	4	drive-N-term-truncate
U6	16	3 (6.1)	3	4	unknown
Sp3	2	4 (8.2)	3	4	unknown
Foxj3	4	4 (8.2)	3	4	drive-C-term-truncate
Igf1r	7	4 (8.2)	2	4	drive-N-term-truncate
Brwd3	X	3 (6.1)	2	4	enhance-intact
Tmcc3	10	3 (6.1)	2	3	drive-N-term-truncate
Prdm2	4	2 (4.1)	2	3	drive-C-term-truncate

Note: 49 neurofibromas were sequenced from quadruple mice; 14 neurofibromas were sequenced from control mice

B

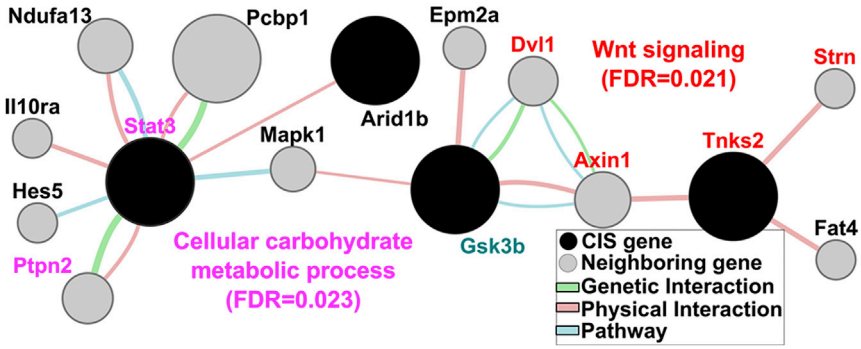

Figure 1. Genes Identified by Sleeping Beauty Transposon System Predict Stat3 and Wnt Pathway Activation in Neurofibroma

(A) Common insertion sites (CISs) identified from neurofibromas. The positions were based on the Ensembl NCBI m37 April 2007 mouse assembly.

(B) Genemania pathway analysis using 22 CIS (black) and 20 genes (gray) connected to CIS by genetic, physical, or Stat3 pathway analysis identifies two significantly deregulated networks. Wnt signaling related gene names are shown in red, and cellular carbohydrate metabolic process related genes are in pink. GSK3b (turquoise) connects these pathways to those in Figure S2. Circle size correlates to network association probabilities.

both. There was a significant correlation between P-STAT3 and total β-catenin (Figures 2E and 2F). Thus, the STAT3 and β-catenin pathways are activated in human neurofibromas and are highly correlated.

Targeted Genetic Deletion of Stat3 in SCs and SCPs Decreases Neurofibroma Numbers and Delays Neurofibroma Formation In Vivo

We then tested whether activation of Stat3 in SCs and SCPs is necessary for neurofibroma initiation and/or maintenance. Loss of Stat3 in *Stat3*$^{fl/fl}$;*DhhCre* mice had no influence on peripheral (saphenous) nerve structure, as shown by electron microscopy; Remak bundles and myelinated axons showed normal differentiated morphology (Figures S2A and S2B). We bred *Stat3*$^{fl/fl}$ mice onto *Nf1*$^{fl/fl}$;*DhhCre* mice; this required generating recombinants, as both *Nf1* and *Stat3* reside on mouse chromosome 11. Kaplan-Meier survival analysis revealed a significant difference in mouse survival between *Stat3*$^{fl/fl}$;*Nf1*$^{fl/fl}$;*DhhCre* mice and *Stat3*$^{fl/+}$;*Nf1*$^{fl/fl}$;*DhhCre* mice ($p < 0.001$) or between *Stat3*$^{fl/fl}$;*Nf1*$^{fl/fl}$;*DhhCre* mice and *Nf1*$^{fl/fl}$;*DhhCre* mice ($p < 0.001$). Loss of one Stat3 allele does not influence survival (*Stat3*$^{fl/+}$;*Nf1*$^{fl/fl}$;*DhhCre* mice versus *Nf1*$^{fl/fl}$;*DhhCre* mice; $p = 0.66$) (Figure 3A).

Nf1$^{fl/fl}$;*DhhCre* nerves continually and significantly increased in size, corresponding to neurofibroma initiation and neurofibroma growth reported in this model (Wu et al., 2008). Representative tumors at 9 months are shown in a *Nf1*$^{fl/fl}$;*DhhCre* versus a *Stat3*$^{fl/fl}$;*Nf1*$^{fl/fl}$;*DhhCre* mouse (Figure 3B). We quantified total neurofibroma burden by volumetric measurement of MRI scans, followed by mixed effects analysis of tumor volume. Strikingly, double mutant nerves (average, 20 mm^3) were similar to WT nerves (8–19 mm^3) (Figure 3C). The difference between controls (*Nf1*$^{fl/fl}$;*DhhCre* or *Stat3*$^{fl/+}$;*Nf1*$^{fl/fl}$;*DhhCre*; n = 9) and *Stat3*$^{fl/fl}$;*Nf1*$^{fl/fl}$;*DhhCre* mice (n = 15) was significant ($p < 0.001$ at 4, 7, and 9 months; Figures S2C and S2D).

In the *Nf1*$^{fl/fl}$;*DhhCre* model, each mouse develops 4–20 neurofibromas. If Stat3 contributes to neurofibroma initiation, then tumor number should be reduced in Stat3 mutants. Indeed, *Stat3*$^{fl/fl}$;*Nf1*$^{fl/fl}$;*DhhCre* mice had significant fewer tumors per mouse versus *Stat3*$^{fl/+}$;*Nf1*$^{fl/fl}$;*DhhCre* littermates upon spinal cord dissection in 5-month-old mice (Figure 3D). Confirming volumetric MRI scan results, the neurofibroma diameter measured at spinal roots upon dissection was significantly smaller in *Stat3*$^{fl/fl}$;*Nf1*$^{fl/fl}$;*DhhCre* versus *Stat3*$^{fl/+}$;*Nf1*$^{fl/fl}$;*DhhCre* mice (Figure 3E). Rare small neurofibromas showed hyperplasia or GEM grade 1 neurofibroma histology (Figure S3). Ki67$^+$ proliferating cells in neurofibroma tissue sections significantly decreased in *Stat3*$^{fl/fl}$;*Nf1*$^{fl/fl}$;*DhhCre* neurofibromas (Figure 3F); numbers of dying cells were unchanged (CC3+) (Figure 3G). Importantly, Stat3 protein was absent in flow-cytometry-sorted EGFP$^+$ SCPs and SCs from *Stat3*$^{fl/fl}$;*Nf1*$^{fl/fl}$;*DhhCre;EGFP*$^+$ mice (Figure 3H); we did, however, detect increased levels of Stat1 and Stat5 (data

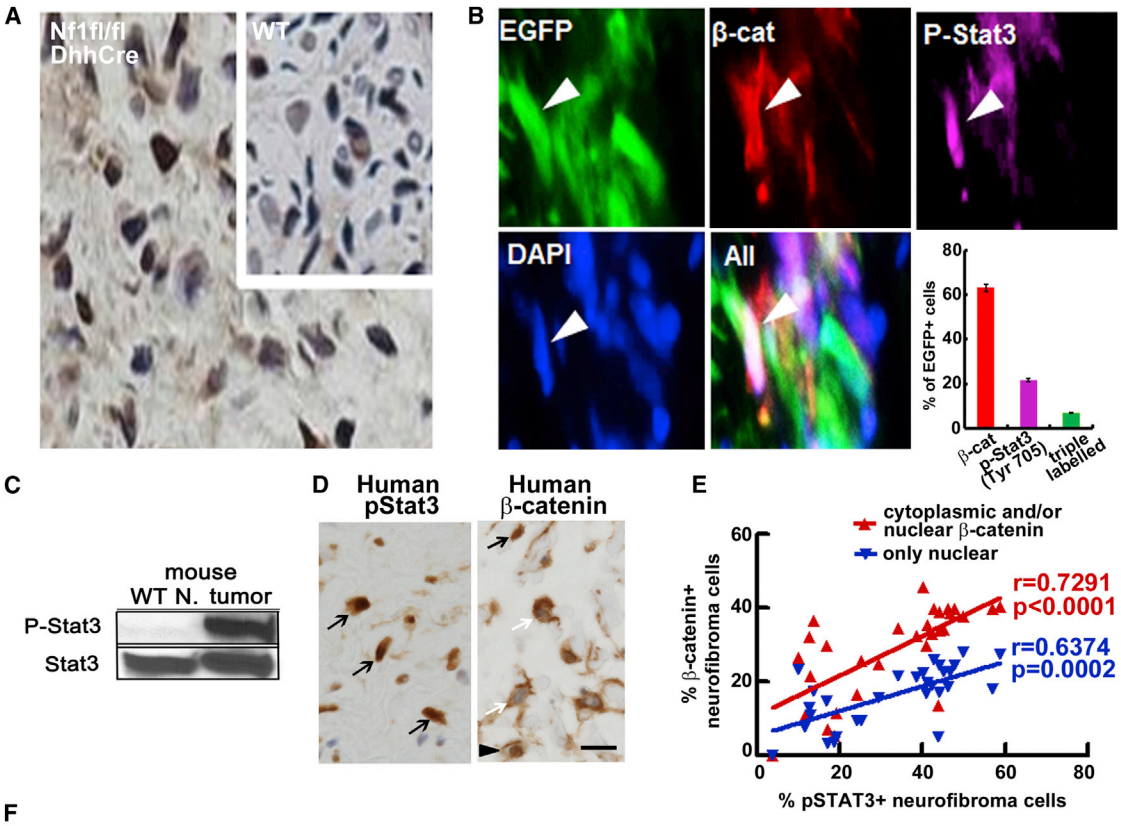

F

	% tumors with P-STAT3 staining			% tumors with β-catenin staining		
Staining Intensity	negative	low	med-high	negative	low	med-high
Plexiform neurofibroma (n=30)	3.3	40	56.7	3.3	36.7	60
Correlation coefficient	0.4373					
P value (two-tailed)	0.0157					

Figure 2. P-STAT3 and β-catenin Expression Correlate in Mouse and Human Neurofibromas

(A) P-Stat3 immunostaining in mouse neurofibromas and WT sciatic nerves (inset), visualized with DAB (brown). Nuclei are counterstained with hematoxylin (blue).

(B) Representative immunofluorescent images show EGFP$^+$ SCs (white arrows); some are also P-Stat3$^+$ (purple) and β-catenin$^+$ (red). Neurofibromas from three mice (four sections per tumor) were stained. 350–500 EGFP$^+$ cells were counted per section. DAPI (blue) staining highlights nuclei. Mean ± SEM is shown.

(C) Western blot of P-Stat3-Y705 (P-Stat3) and total Stat3 (Stat3) in mouse neurofibroma (tumor) and WT sciatic nerve (WT nerve); blot is representative of neurofibromas (n = 5) and WT nerves (n = 3).

(D) Representative pictures of immunostaining of P-STAT3(Y705) (left) and β-catenin (right) in human plexiform neurofibroma. On the right, the black arrow indicates nuclear β-catenin, the white arrows indicate cytoplasmic β-catenin, and the black arrowhead indicates both. Scale bar, 10 μm.

(E) Distribution of % P-STAT3 positive neurofibroma cells versus % nuclear β-catenin positive only (blue) or cytoplasmic and/or nuclear β-catenin positive (red) in 30 human plexiform neurofibromas. Spearman correlation coefficient analysis between P-STAT3(Y705) and β-catenin distribution (P-STAT3 versus total beta catenin shown in red, r = 0.7219, p < 0.0001; P-STAT3 versus nuclear beta catenin shown in blue, r = 6374, p = 0.0002, two-tailed).

(F) Quantification of intensity of P-STAT3(Y705) and β-catenin immune-positive cells in NF1 human plexiform neurofibromas and Spearman correlation coefficient analysis between P-STAT3(Y705) and β-catenin intensity (r = 0.4373; p = 0.0157, two-tailed).

not shown). Therefore, glial cell Stat3 regulates tumor cell proliferation in neurofibromas, and activation of Stat3 in SCs and/or SCPs is important for neurofibroma initiation and growth.

Stat3 Contributes to Neurofibroma Initiation

Our in vivo analyses could not distinguish function(s) of P-Stat3 in neurofibroma SCs versus SCPs, because the genetic loss of function targets both. To confirm that Stat3 is relevant to neurofibroma SCP-like cells, we used sphere culture, enabling detection of growth and self-renewal of nervous system stem and/or progenitors. We isolated cells directly from human plexiform neurofibromas and cultured them as floating spheres at clonal density. We blocked STAT3 signaling with FLLL32, a JAK2/STAT3 inhibitor (Lin et al., 2010). FLLL32 inhibited human neurofibroma sphere formation (IC_{50}, 0.3 μM) (Figures 4A and 4B). Western blot confirmed decreased STAT3-Y705 phosphorylation and slightly reduced total STAT3 (Figure 4C).

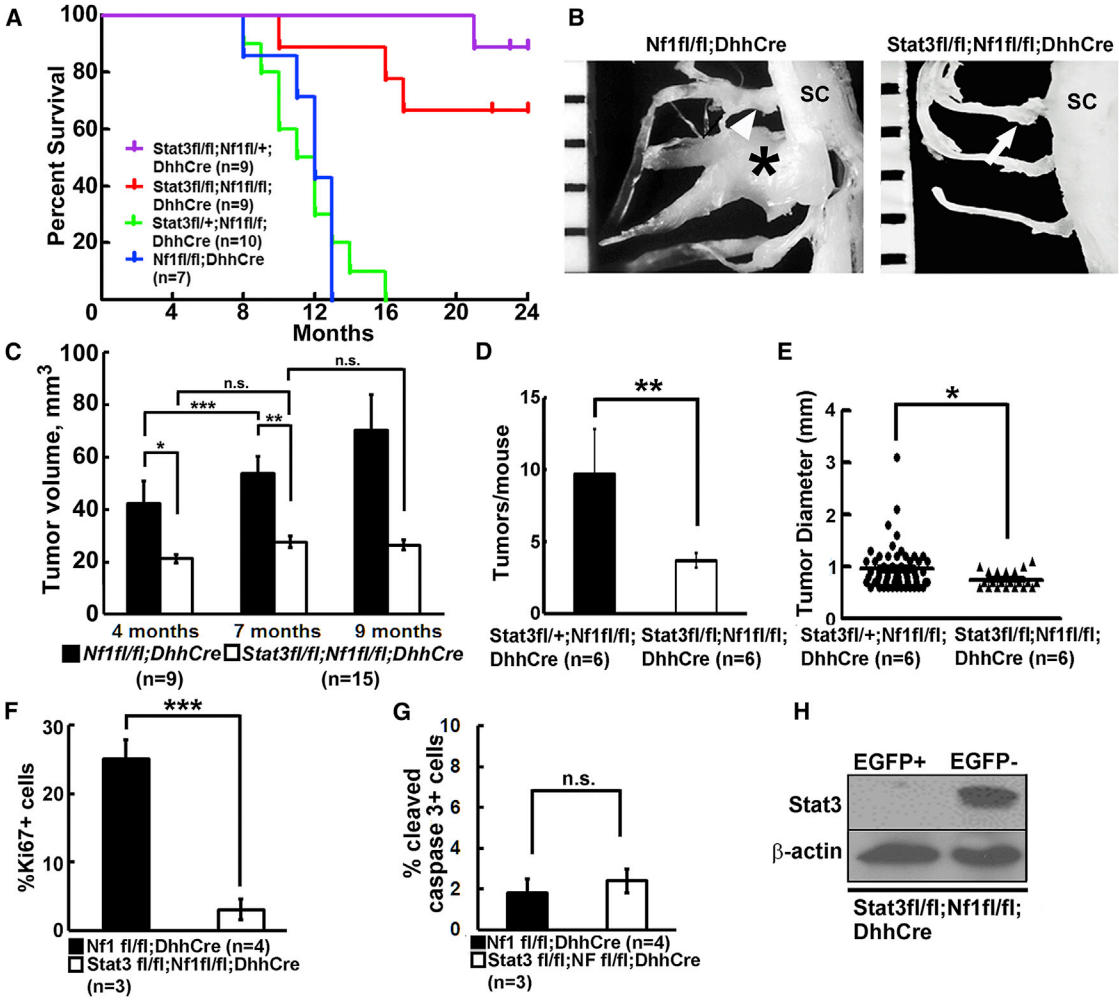

Figure 3. Targeted Genetic Deletion of Stat3 in SCs and SCPs Delays Neurofibroma Formation In Vivo

(A) Kaplan-Meier survival curve. Purple: *Stat3* $^{fl/fl}$*;Nf1*$^{fl/+}$*;DhhCre*. Red: *Stat3*$^{fl/fl}$*;Nf1*$^{fl/fl}$*;DhhCre*. Blue: *Stat3* $^{fl/+}$*;Nf1*$^{fl/fl}$*;DhhCre*. Green: *Nf1*$^{fl/fl}$*;DhhCre*.

(B) Representative gross dissections of thoracic paraspinal neurofibromas and nerve roots in 9-month-old *Nf1*$^{fl/fl}$*;DhhCre* (left) and *Stat3*$^{fl/fl}$*;Nf1*$^{fl/fl}$*;DhhCre* (right) mice. The ruler shows 1-mm markings.

(C) Neurofibroma volumes at 4, 7, and 9 months of age, measured in MRI images. *Nf1*$^{fl/fl}$*;DhhCre* mice (n = 12, black bars) and *Stat3*$^{fl/fl}$*;Nf1*$^{fl/fl}$*;DhhCre* mice (n = 15, white bars) at 4, 7, and 9 months of age are shown.

(D) Average tumor number per mouse at 5 months in the *Stat3*$^{fl/fl}$*;Nf1*$^{fl/fl}$*;DhhCre* (white bar, n = 6) and littermates *Stat3*$^{fl/+}$*;Nf1*$^{fl/fl}$*;DhhCre* mice (black bar, n = 6).

(E) Tumor diameter in the *Stat3*$^{fl/fl}$*;Nf1*$^{fl/fl}$*;DhhCre* (circle, n = 6 mice with 57 tumors) and littermates *Stat3*$^{fl/+}$*;Nf1*$^{fl/fl}$*;DhhCre* mice (triangle, n = 6 mice with 21 tumors).

(F) Cell proliferation shown as percent Ki67$^+$ cells in *Nf1*$^{fl/fl}$*;DhhCre* mice (n = 4, black bar) and *Stat3*$^{fl/fl}$*;Nf1*$^{fl/fl}$*;DhhCre* mice (n = 3, white bar).

(G) Cell death shown as percent cleaved caspase 3$^+$ cells in *Nf1*$^{fl/fl}$*;DhhCre* mice (n = 4, black bar) and *Stat3*$^{fl/fl}$*;Nf1*$^{fl/fl}$*;DhhCre* mice (n = 3, white bar).

(H) Western blot on FACS-sorted EGFP+, EGFP− cells dissociated from adult *Stat3*$^{fl/fl}$*;DhhCre;EGFP*$^{fl/fl}$ mouse sciatic nerves.

Statistics: ordinary one-way ANOVA (C) and unpaired Student's t test (D–G). * = $p < 0.05$, ** = $p < 0.01$, *** = $p < 0.001$, n.s. = not significant.

Importantly, FLLL32 inhibited the formation of *Nf1*$^{-/-}$ SCP spheres (IC_{50}, 0.5–1 μM), yet affected WT SCPs only at 10× higher concentration (Figure 4D). We also dissociated dorsal root ganglia (DRG) and/or early neurofibromas from 6-week-old mice. *Stat3*$^{fl/fl}$*;Nf1*$^{fl/fl}$*;DhhCre* cells formed significantly fewer primary and secondary spheres than *Nf1*$^{fl/fl}$*;DhhCre* cells (Figures 4E and 4F); sphere size was similar (data not shown). We also depleted *Stat3* from *Nf1*$^{fl/fl}$*;DhhCre* neurofibroma SCP spheres with short hairpin RNA (shRNA). Sphere numbers were significantly reduced 4 days after shStat3 infection, versus non-target controls (Figure S4A); we confirmed decreased Stat3 by western blot (Figure S4B). Thus, Stat3 increases *Nf1* mutant SCP self-renewal. In many cancers, self-renewing stem and/or progenitor-like cells contribute to tumorigenesis. Neurofibroma-like lesions were detected in seven out of eight *nu/nu* mice that were subcutaneously transplanted with *Nf1*$^{fl/fl}$*;DhhCre* mice derived sphere cells (Figures 4G and 4H), while no lesion was detected in *Stat3*$^{fl/fl}$*;Nf1*$^{fl/fl}$*;DhhCre* derived sphere cells (Figure 4G). H&E staining of tissue sections showed no features of malignancy (Figure 4I) and anti-S100β$^+$

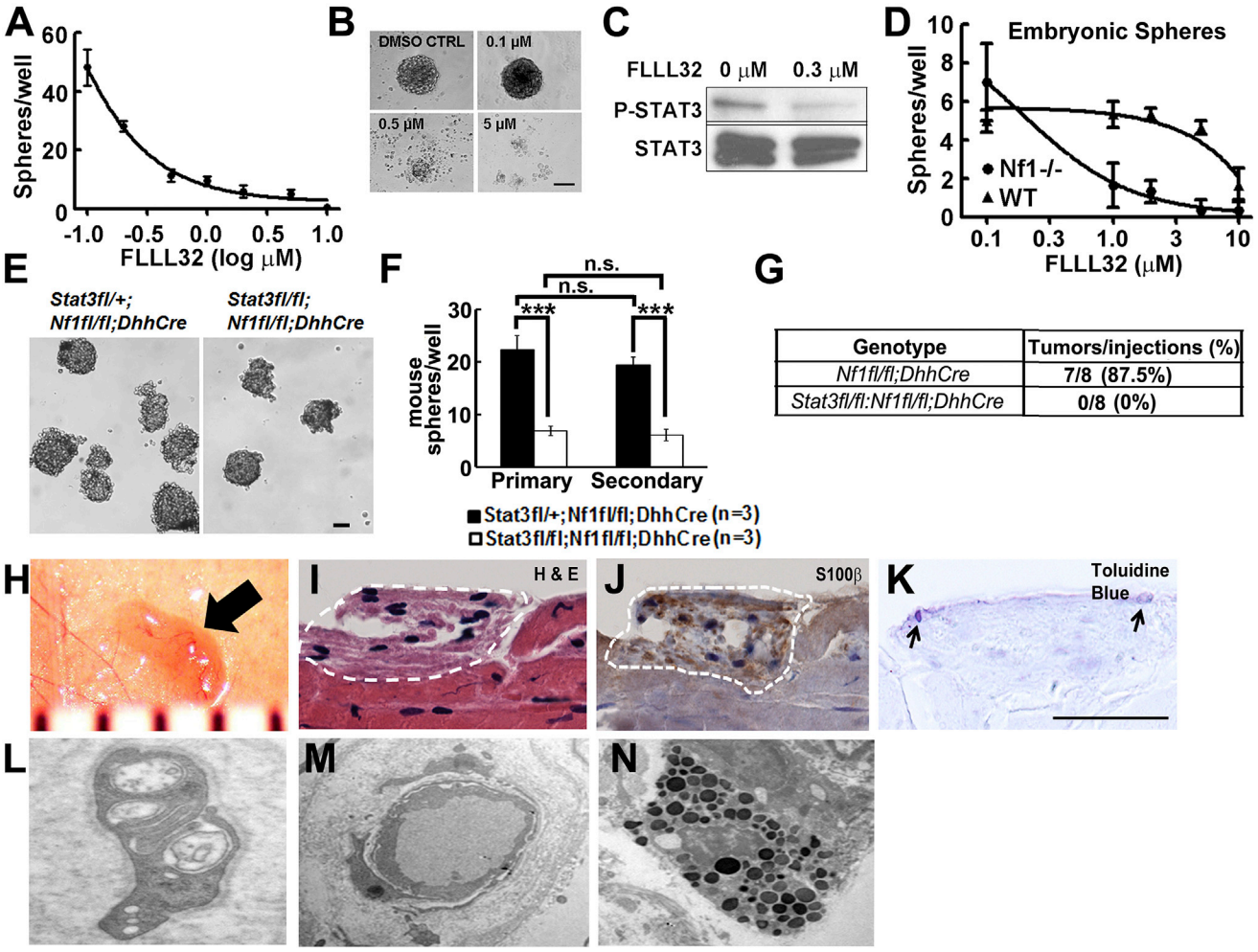

Genotype	Tumors/injections (%)
Nf1fl/fl;DhhCre	7/8 (87.5%)
Stat3fl/fl:Nf1fl/fl;DhhCre	0/8 (0%)

Figure 4. Stat3 Contributes to Neurofibroma Initiation

(A) The JAK2/STAT3 inhibitor FLLL32 inhibits formation of human neurofibroma spheres. DMSO (0) served as control.

(B) Phase contrast images of human neurofibroma spheres treated with FLLL32 for 5 days.

(C) Western blot of P-STAT3-Y705 and STAT3 in human neurofibroma spheres, ±0.3 μM FLLL32.

(D) Low doses of FLLL32 inhibit formation of mouse E12.5 *Nf1*$^{-/-}$ spheres; effects on E12.5 WT spheres are observed only at higher concentrations.

(E) Phase contrast images of primary neurofibroma and/or DRG spheres from *Stat3*$^{fl/+}$;*Nf1*$^{fl/fl}$;*DhhCre* mice (left; control) and *Stat3*$^{fl/fl}$;*Nf1*$^{fl/fl}$;*DhhCre* mice (right).

(F) Primary and secondary neurofibroma and/or DRG sphere number is reduced in the absence of Stat3 (n = 3 per group).

(G) Neurofibroma-like lesions form after subcutaneous injection of *Nf1*$^{fl/fl}$;*DhhCre* neurofibroma sphere cells but not in *Stat3*$^{fl/fl}$;*Nf1*$^{fl/fl}$;*DhhCre* mouse derived neurofibroma sphere cells.

(H) Gross photograph of a lesion (black arrow) under reflected skin in a mouse injected with *Nf1*$^{fl/fl}$;*DhhCre* neurofibroma sphere cells. The ruler shows 1-mm markings.

(I) H&E stained section of (F); lesion is indicated by white dotted line.

(J) Immunohistochemistry showing S100β^{+} cells (brown) in tumor. Blue: hematoxylin counterstain.

(K) Toluidine blue staining showing mast cells (black arrows).

(L, M, and N) EM showing that lesions contain SCs, identified by continuous basal lamina and wrapping of small axons (L), blood vessels (M), and mast cells (N). Scale bars, 50 μm (B and E) and 20 μm (K). Statistics: ordinary one-way ANOVA.

cells SCs (Figure 4J) and mast cells (Figure 4K). Electron microscopy (EM) demonstrated that these lesions contained SCs identified by their continuous basal lamina and wrapping of small axons (Figure 4L), blood vessels (Figure 4M), and mast cells (Figure 4N)—all features of neurofibroma. These in vitro and in vivo genetic results support the conclusion that *Nf1*$^{-/-}$ SCP self-renewal and neurofibroma tumorigenic potential are regulated by Stat3.

Stat3 Activates β-catenin Signaling

Data in Figures 1 and 2 suggest a Stat3-β-catenin link in neurofibroma SCs. Stabilized β-catenin translocates to the nucleus and alters target gene transcription (Liu et al., 2002). *Stat3*$^{fl/fl}$;*Nf1*$^{fl/fl}$;*DhhCre* neurofibromas showed significantly decreased active (nuclear) β-catenin (45%), increased inactive β-catenin (P-β-catenin, S33, S37, and T41) (591% in cytoplasm, 166% in nucleus), and decreased cyclin D1 expression (>90%) in

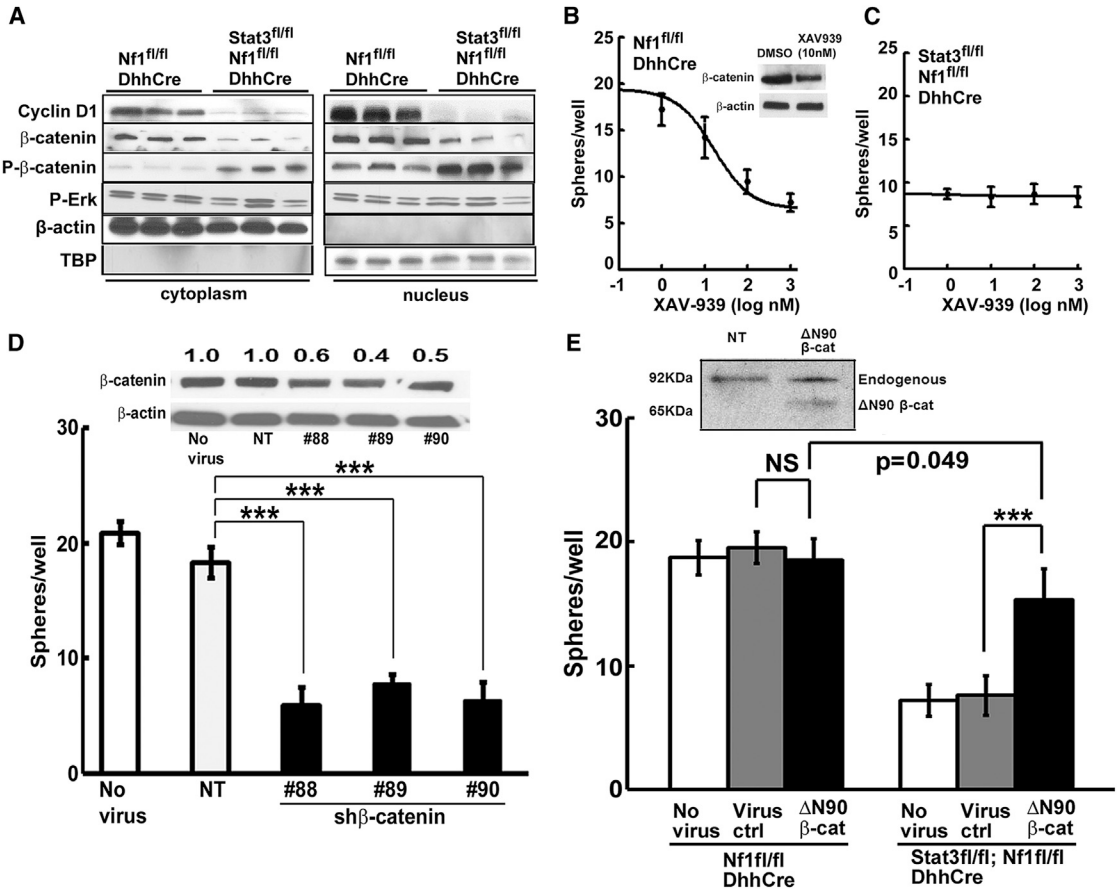

Figure 5. β-catenin Signaling Is a Critical Indicator of Stat3 in Neurofibromas

(A) Western blots of nuclear and cytoplasmic proteins from *Stat3*$^{fl/fl}$;*Nf1*$^{fl/fl}$;*DhhCre* or *Nf1*$^{fl/fl}$;*DhhCre* mouse neurofibromas and/or DRGs with indicated antibodies.

(B) β-catenin tankyrase inhibitor XAV-939 inhibits formation of *Nf1*$^{fl/fl}$;*DhhCre* mouse neurofibroma spheres. DMSO (0) was the control. Inset: 10 nM XAV-939 inhibited β-catenin expression by 3 days is shown.

(C) Low dose XAV-939 has no effect on the formation of *Stat3*$^{fl/fl}$;*Nf1*$^{fl/fl}$;*DhhCre* mouse neurofibroma spheres.

(D) Three shβ-catenin shRNA (#88, #89, and #90) each decrease mouse neurofibroma sphere formation, versus non-target lentivirus YFP (NT) or no virus controls. The inset shows western blot confirming shβ-catenin-mediated knockdown of total β-catenin. Anti-β-actin is the loading control. Numbers show the ratio of β-catenin to β-actin loading control, then to no virus expression level.

(E) Overexpression of β-catenin deltaN90 (ΔN90) in *Stat3*$^{fl/fl}$;*Nf1*$^{fl/fl}$;*DhhCre* mouse neurofibroma and/or DRG spheres increased sphere numbers (black) versus virus (gray, $p < 0.001$) or no virus controls (white, $p < 0.001$). Overexpression of ΔN90 β-catenin in *Nf1*$^{fl/fl}$;*DhhCre* mouse neurofibroma and/or DRG spheres did not significantly increase sphere numbers (black) versus virus (gray, $p = 0.15$) or no virus (white, $p = 0.43$). Inset: western blot detects endogenous 92KDa β-catenin and ~60 KDa of overexpression of mutated ΔN90 catenin in *Stat3*$^{fl/fl}$;*Nf1*$^{fl/fl}$;*DhhCre* mouse neurofibroma spheres.

Statistics: ordinary one-way ANOVA. Three independent experiments were performed in (B), (C), and (E).

cytoplasm and nucleus versus controls (Figure 5A). In contrast, P-Erk did not change (Figure 5A). Thus, neurofibroma β-catenin expression, localization, and target gene expression are regulated by Stat3.

To verify this conclusion in a system amenable for mechanistic analysis, we isolated SCPs from *Nf1*$^{fl/fl}$;*DhhCre* neurofibromas and cultured them with or without blocking β-catenin signaling with the tankyrase inhibitor XAV-939, which stabilizes axin, a component of the β-catenin destruction complex. XAV-939 inhibited mouse neurofibroma sphere formation (IC_{50}, 0.1 μM). Western blot confirmed a 50% decrease in total β-catenin with 3 days of drug exposure (10 nM) (Figure 5B). Supporting the hypothesis that Stat3 is critical for β-catenin expression, remarkably, *Stat3*$^{fl/fl}$;*Nf1*$^{fl/fl}$;*DhhCre* mouse neurofibroma spheres were insensitive to 100× higher concentrations of XAV-939 (Figure 5C). Depleting β-catenin with shRNA in *Nf1*$^{fl/fl}$;*DhhCre* neurofibroma SCP-like spheres also significantly reduced sphere numbers versus controls (Figure 5D); we confirmed decreased β-catenin by western blot (Figure 5D, inset). Thus, β-catenin stabilization requires Stat3 in *Nf1*$^{-/-}$ neurofibroma derived SCP-like cells.

If β-catenin is critical in Stat3-driven neurofibromagenesis, then *Stat3*$^{fl/fl}$;*Nf1*$^{fl/fl}$;*DhhCre* spheres, which do not form tumors, should be rescued by β-catenin. To test this, we infected spheres with a stable, active β-catenin mutant (ΔN90 β-catenin) or virus control. Remarkably, overexpression of

ΔN90 β-catenin significantly increased the number of *Stat3*$^{fl/fl}$;*Nf1*$^{fl/fl}$;*DhhCre*, but not *Nf1*$^{fl/fl}$;*DhhCre*, neurofibroma spheres (Figure 5E). Importantly, seven out of nine mice injected with ΔN90 β-catenin infected *Stat3*$^{fl/fl}$;*Nf1*$^{fl/fl}$;*DhhCre* spheres developed neurofibroma-like lesions, while no lesions were detected in vector controls. Thus, β-catenin is a major effector of Stat3 signaling in SCP and is necessary for neurofibromagenesis.

Stat3 Alters Gsk3β Inhibitory Phosphorylation

We wondered how Stat3 activates β-catenin in neurofibromas. *Gsk3β* was a frequent CIS identified in our insertional mutagenesis screen, which predicted reduced GSK3β (Figure 1). GSK3β(Ser9) phosphorylation inhibits GSK3β activity, allowing β-catenin stabilization or activation (Wu and Pan, 2010). *STAT3* can negatively regulate GSK3β transcription (Moh et al., 2008). *Gsk3β* mRNA expression increased in *Stat3*$^{fl/fl}$;*Nf1*$^{fl/fl}$;*DhhCre* versus *Nf1*$^{fl/fl}$;*DhhCre* neurofibromas (Figure S5A), supporting the idea that Stat3 transcriptionally represses Gsk3β in neurofibromas. Chromatin immunoprecipitation (ChIP) using anti-Stat3 detected Stat3 bound to the Stat3 binding motif in the *Gsk3β* 5′ UTR in neurofibroma DNA (Figures S5B and S5C). Furthermore, in the absence of Stat3 total Gsk3β increased in neurofibromas (Figure S5D). Thus, in neurofibromas Stat3 represses *Gsk3β* transcription, correlating with a reduction in Gsk3β protein. However, targeting *Gsk3β* with shRNA only slightly rescued sphere formation in *Stat3*$^{fl/fl}$;*Nf1*$^{fl/fl}$;*DhhCre* SCP spheres (Figure S5E), suggesting the existence of additional pathways.

Stat3 Transcriptionally Represses *Arid1b* Expression

Arid1b was another frequent CIS identified by insertional mutagenesis (Figure 1A). Transposon insertions into the *Arid1b* locus predicted disrupted C termini or truncated N termini, e.g., inactivating insertions, and anti-Arid1b immunofluorescence was strong in WT SCs but reduced in neurofibroma SCs (Figure S6A). qRT-PCR confirmed negative regulation of *Arid1b* mRNA expression in neurofibromas by Stat3 (e.g., *Arid1b* mRNA is low in neurofibromas and increases in the absence of *Stat3*; Figure 6A). Similar results were observed in fluorescence-activated cell sorting (FACS)-sorted EGFP^{+} neurofibroma SCs versus WT SCs (Figure S6B). We identified a putative Stat3 binding site 7 kb downstream of the mouse *Arid1b* transcriptional start site (Figures 6B and S7). When *Nf1*$^{fl/fl}$;*DhhCre* neurofibroma DNA was subjected to ChIP using anti-Stat3, we detected Stat3 bound to *Arid1b* at this site by PCR (Figure 6C).

Arid1b expression was low in *Nf1*$^{fl/fl}$;*DhhCre* and high in *Stat3*$^{fl/fl}$;*Nf1*$^{fl/fl}$;*DhhCre* tumor-derived neurofibroma spheres (data not shown). We exposed *Stat3*$^{fl/fl}$;*Nf1*$^{fl/fl}$;*DhhCre* neurofibroma spheres to sh*Arid1b*. Decreasing *Arid1b* expression significantly increased sphere numbers (Figure 6D), correlating with elevated levels of activated β-catenin protein (Figure 6E) and mRNA expression (Figure 6F), and elevated levels of the β-catenin target genes *Axin2*, *Ccnd1*, and *Myc* (Figure 6F). sh*Gsk3β* increased β-catenin and its target gene mRNA expression in *Stat3*$^{fl/fl}$;*Nf1*$^{fl/fl}$;*DhhCre* spheres (Figure 6G) but did not rescue numbers of *Stat3*$^{fl/fl}$;*Nf1*$^{fl/fl}$;*DhhCre* spheres (Figures 7Band S5E). Knockdown of *Gsk3β* and *Arid1b* simultaneously with shRNA showed similar effects to sh*Arid1b* alone (Figure 7A).

To test whether tumor formation is affected by reduction in *Arid1b*, *Gsk3β*, or both, we transplanted sphere cells into nude mice. *Stat3*$^{fl/fl}$;*Nf1*$^{fl/fl}$;*DhhCre* spheres rarely formed tumors. Tumors formed in *Stat3*$^{fl/fl}$;*Nf1*$^{fl/fl}$;*DhhCre* sphere cells infected with sh*Gsk3β*, sh*Arid1b*, or sh*Arid1b* + sh*Gsk3β* by 8 weeks after transplantation ($p = 0.0157$; Figure 7B). There were no significant differences between the three experimental groups ($p = 0.3669$), suggesting both *Gsk3β* and *Arid1b* are involved in *Stat3*-mediated neurofibromagenesis.

ARID1B acts in SWI/SNF complexes containing BRG1, the central catalytic subunit of numerous chromatin-modifying enzymatic complexes (Trotter and Archer, 2008). BRG1 can be required for Stat3 recruitment to target genes (Ni and Bremner, 2007). To test whether Arid1b requires Brg1 to affect sphere numbers, we knocked down *Brg1* and/or *Arid1b* in *Stat3*$^{fl/fl}$;*Nf1*$^{fl/fl}$;*DhhCre* spheres with shRNA. The low numbers characteristic of *Stat3*$^{fl/fl}$;*Nf1*$^{fl/fl}$;*DhhCre* spheres were rescued by sh*Arid1b*, but not sh*Brg1*. The combination of sh*Arid1b* together with sh*Brg1* prevented the sh*Arid1b* effect, indicating that the effect requires Brg1 and most likely chromatin remodeling (Figure 7C).

Stat3 binds the Arid1b promoter fragment, repressing *Arib1b* expression. Arid1b's known function is in chromatin remodeling, and we wondered if the *Arid1b* gene itself might be subject to Stat3-dependent histone modification. We performed ChIP with antibodies recognizing the histone modifications H3K4Me3, H3K9Me2, and H3K9Ac in vehicle or Stat3 inhibitor (FLLL32) treated primary mouse neurofibroma SCs at the *Arid1b* promoter. We detected a significant enhancement in the $H3K4Me_3$ marks at the *Arid1b* promoter in three independent experiments ($p < 0.05$). In contrast, $H3K9Me_2$ or H3K9Ac did not significantly change at this site after FLLL32 exposure (Figure 7D). Taken together, in the setting of *Nf1* loss, Stat3 transcriptionally represses the SWI/SNF gene *Arid1b* through histone $H3K4Me_3$ modification and this repression is BRG1 dependent (Figure 7E). This results in an increase in β-catenin.

DISCUSSION

By performing an unbiased insertional mutagenesis screen and using mouse genetics and SCP culture, we identified an Nf1/P-Stat3/Arid1b/β-catenin pathway in SCP that is critical for neurofibroma initiation. P-Stat3 is a major neurofibroma oncogene as targeted genetic deletion of *Stat3* in nerve SCs and SCPs dramatically delays neurofibroma formation and tumors, once formed, grow very slowly (Figures 2A–2C). *Stat3* provides a first example of a genetic loss of function affecting neurofibroma initiation and growth in vivo. Loss of *Stat3* decreased numbers of neurofibroma SCP-like cells, neurofibroma SCP self-renewal, and neurofibroma formation by SCP after transplantation, functions defining cancer stem- and/or progenitor-like cells in tumor initiation (Figure 4). Importantly, β-catenin expression rescued all phenotypes driven by Stat3 loss of function in *Nf1* mutant SCPs (Figure 5E). Supporting the relevance of

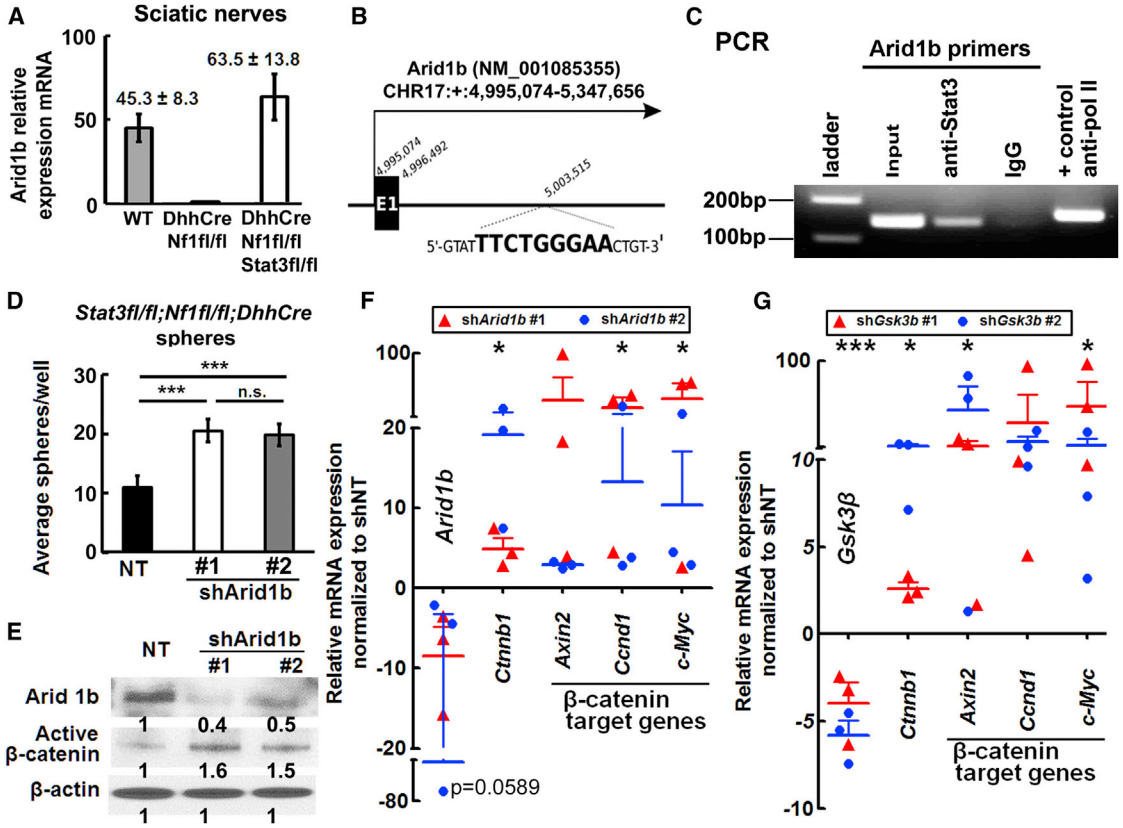

Figure 6. Stat3 Transcriptionally Represses Arid1b Expression, Activating β-catenin

(A) qRT-PCR shows high *Arid1b* mRNA in *Stat3*$^{fl/fl}$;*Nf1*$^{fl/fl}$;*DhhCre* mouse sciatic nerve (white, n = 6) versus WT (n = 6) and *Nf1*$^{fl/fl}$;*DhhCre* nerve (n = 6).

(B) Schematic, exon 1 mouse *Arid1b* gene. A putative Stat3 binding motif is between Exon 1 and Exon 2; the binding motif sequence is shown in bold.

(C) Stat3 on the *Arid1b* promoter. PCR amplified a 139-bp *Arid1b* DNA fragment after ChIP with anti-Stat3. IgG was the negative control.

(D) Two *Arid1b* shRNA increase the number of *Stat3*$^{fl/fl}$;*Nf1*$^{fl/fl}$;*DhhCre* mouse neurofibroma spheres.

(E) Western blot shows knockdown of Arid1b and increased β-catenin in *Stat3*$^{fl/fl}$;*Nf1*$^{fl/fl}$;*DhhCre* mouse neurofibroma spheres 4 days after sh*Arid1b* infection in two different shRNA clones.

(F and G) β-catenin target gene expression increases after sh*Arid1b* (F) or sh*Gsk3β* (G) infection of *Stat3*$^{fl/fl}$;*Nf1*$^{fl/fl}$;*DhhCre* neurofibroma spheres.

Mean ± SEM is shown for three independent experiments and two clones of shRNA in (D), (F), and (G). A representative experiment (of three) is shown in (C). Statistics: ordinary one-way ANOVA.

our findings to human neurofibromas, primary patient-derived neurofibroma SCP-like cell sphere formation, a surrogate of tumor initiation, was dramatically reduced by Jak2/Stat3 inhibition (Figure 4A), and P-Y705-STAT3 and β-catenin expression were highly correlated in human plexiform neurofibromas (Figure 2).

We confirmed that Stat3 and β-catenin are detectable in human plexiform neurofibromas and demonstrated that Stat3 and β-catenin are critical for neurofibroma formation in transplantation (Figure 5G). The Sleeping Beauty system and pathway analysis defined mutations predicting loss of *Gsk3β* and *Arid1b*, identifying the *WNT* and *STAT* pathways as players that might cooperate with loss of *Nf1* in neurofibromagenesis (Figure 1). GSK3β and β-catenin signaling were previously implicated in MPNST, sarcomas that are malignant derivatives of neurofibromas (Mo et al., 2013; Rahrmann et al., 2013; Watson et al., 2013). Other CIS genes (*WAPAL*, *SP3*, *BTBD9*, and *IGFR1*) are upregulated in neurofibroma cells, suggesting roles as proto-oncogenes early in tumor progression. Downregulated CIS genes (*TMCC3*, *SLC35F1*, and *SORCS*) may have tumor suppressor functions.

Stat3 is present on the *Gsk3β* promoter in neurofibromas (Figure S5), consistent with Stat3 repressing GSK3β transcription in hepatocytes (Moh et al., 2008). In SCP, decreasing *Gsk3β* also increased β-catenin target gene expression, and tumor formation, but did not rescue SCP sphere formation. Given that sh*Gsk3β* or *shArid1b* enable tumor formation and β-catenin expression, but only sh*Arid1b* rescues neurofibroma sphere numbers, these genes likely use different mechanisms to repress β-catenin function; loss of either is sufficient to drive neurofibroma formation in the absence of Stat3, suggesting that interference with β-catenin signaling by one of several mechanisms will interfere with tumor formation.

We identify *Arid1b* as a critical link between P-Stat3 and β-catenin. *ARID1B* is a tumor suppressor, mutated by deletion, in neuroblastoma (Sausen et al., 2013). The *ARID1B* promoter can be hyper-methylated, resulting in decreased *ARID1B*

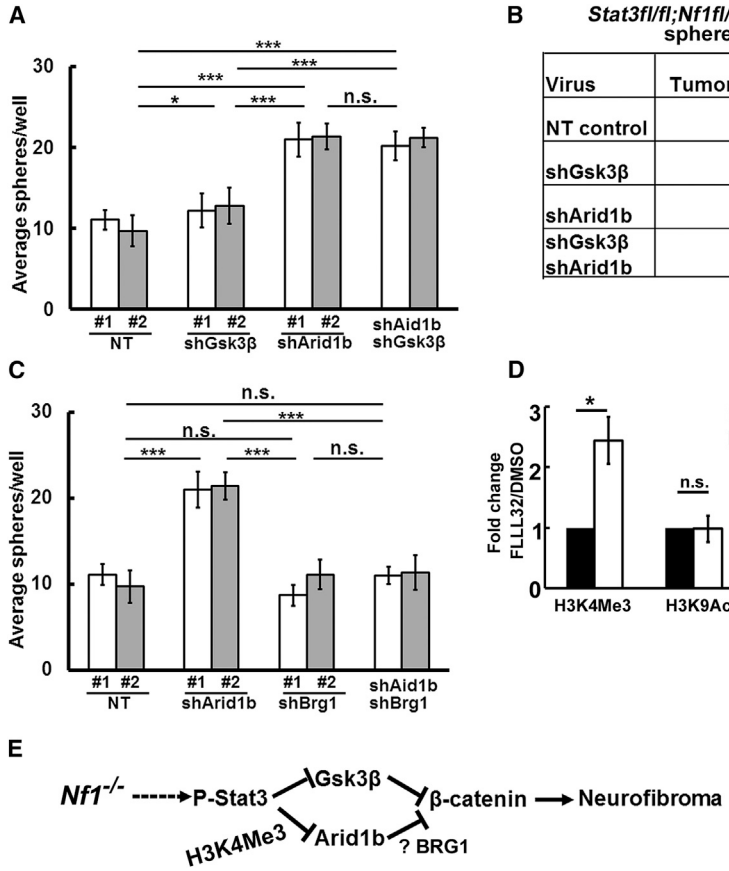

Figure 7. *Arid1b* and *Gsk3β* Contribute to Stat3 Mediated Neurofibromagenesis

(A) In vitro, sh*Gsk3β* does not fully rescue *Stat3*$^{fl/fl}$;*Nf1*$^{fl/fl}$;*DhhCre* sphere numbers. Simultaneous knockdown of *Gsk3β* and *Arid1b* shows similar effects to sh*Arid1b* alone.

(B) Neurofibroma-like tumors form in *Stat3*$^{fl/fl}$;*Nf1*$^{fl/fl}$;*DhhCre* sphere cells infected with sh*Arid1b*, sh*Gsk3β*, or both and transplanted into *nu/nu* mice.

(C) Brg1 is necessary for *Stat3*$^{fl/fl}$;*Nf1*$^{fl/fl}$;*DhhCre* sphere formation in cells treated with sh*Arid1b*.

(D) ChIP shows enhancement of the H3K4Me3 mark at the *Arid1b* promoter.

(E) Schematic shows a model of neurofibroma initiation; loss of *Nf1* in SCP causes activation of P-Stat3. P-Stat3 transcriptionally represses *Arid1b* and *Gsk3β*, increasing β-catenin activity.

Mean ± SEM is shown for three independent experiments in (A), (C), and (D). Two different shRNA clones (#1 and #2) were used in (A) and (C). For combination, we used sh*Arid1b* #1+sh*Gsk3β* #1 (white bar) or sh*Arid1b* #2+sh*Gsk3β* #2 (gray bar) in (A). We used sh*Arid1b* #1+sh*Brg1* #1 (white bar) and sh*Arid1b* #2+sh*Brg1* #2 (gray bar) in (C). Statistics: ordinary one-way ANOVA.

expression, as in pancreatic cancer cells (Khursheed et al., 2013). Arid1b also functions as a tumor suppressor in the context of *Nf1* loss, with low expression in neurofibromas resulting in increased β-catenin, Wnt/β-catenin target gene expression, and tumorigenesis (Figure 6). There was variation in the extent of Wnt/β-catenin target gene expression among samples with shRNA exposure, which is likely due to our use of primary cells. The differentiation state of individual cells in spheres and/or different levels of shRNA expression after lentiviral infection may account for this variation. Although our study was nearing completion, Vasileiou et al. (2015) showed that, as in our study, reducing *ARID1B* increases Wnt/β-catenin target gene expression. They also overexpressed *ARID1B* by transient transfection and inhibited Wnt/β-catenin activity in cell lines. We were unable to overexpress *ARID1B*, as the *ARID1B* cDNA is too large for the lentiviral infection required in our primary cells. Nevertheless, together the two studies strongly support critical roles for *ARID1B* in regulation of Wnt/β-catenin activity.

We detected increased H3K4Me$_3$ at the *Arid1b* promoter region after Stat3 inhibition. Given that the Stat3 binding site is in intron 1 of the *Arid1b* gene, it is likely that Stat3 binds to this intronic region and regulates *Arid1b* by antisense transcription, a mechanism by which mammalian genes regulate sense transcription (Faghihi and Wahlestedt, 2009; Magistri et al., 2012). Genome-wide mapping of chromatin modification will be necessary to further clarify this mechanism.

In summary, loss of *Nf1* activates Stat3 SCPs, enabling tumor initiation by repressing the SWI/SNF gene *Arid1b* through histones H3K4Me3 and H3K27Me3 modification, thereby activating β-catenin. Knockdown of Arid1b in Stat3$^{fl/f}$; *Nf1*$^{fl/fl}$;*DhhCre* SCPs by shRNA is sufficient to recue neurofibroma formation in in vivo transplantation. Mouse and human *NF1* mutant cells are significantly more sensitive than their WT counterparts to treatment with a JAK2/STAT3 inhibitor (Figures 4A and 4D), suggesting that a therapeutic window will exist for neurofibroma therapy using JAK/STAT pathway inhibitors now in clinical trials (Lesina et al., 2011). Given that β-catenin targeted therapeutics are not yet proven, blocking β-catenin via STAT or targeting SWI/SNF complexes may be feasible strategies.

EXPERIMENTAL PROCEDURES

Animals

Mice were housed in temperature- and humidity-controlled facilities on 12-hr dark-light cycles with free access to food and water. The animal care and use committees of Cincinnati Children's Hospital Medical Center or University of Minnesota approved all animal procedures. See the Supplemental Experimental Procedures for additional details.

Pyrosequencing and Genemania Analysis

T2/Onc integration sites from 49 neurofibromas were cloned and sequenced using bar-coded primers and linker-mediated PCR, followed by pyrosequencing. Amplicon sequencing using the GS20 Flex pyrosequencing machine (Roche) was performed according to the manufacturer's protocol. Primers used a unique 10-bp barcode-recognition sequence for each tumor sample. After removal of redundant and other non-specific noise as described (Keng et al., 2009), we obtained 6,353 non-redundant insertions. Next, we identified CISs with more Sleeping Beauty mutagenic transposon insertions than

predicted based on Monte Carlo criteria for statistical significance. We defined CISs as regions in the genome with six insertions located within 185 kb of each other, five insertions within 95 kb, four insertions within 35 kb, or three insertions within 5 kb. We used the Genemania algorithm to generate gene-gene association networks (genetic interaction, physical interaction, and pathways), after inputting these CIS. This generated networks, each of which we extended using the top 20 related genes precomputed in the program. These are defined as neighboring genes. We similarly colored genes significantly enriched in a given "biological process" within a Gene Ontology (GO) category, after applying a significance cutoff of FDR < 0.05).

Embryonic and Neurofibroma Sphere Formation and SC Culture

Embryonic mouse spheres dissociated from E12.5 DRG with 0.25% Trypsin 20 min. at 37°C (Mediatech) produced single-cell suspensions with narrow-bore pipettes and a 70-μm strainer (BD-Falcon). For mouse or human neurofibroma spheres, we chopped tissue into 1–3 mm^3 pieces, which were plated in 20 ml L-15 (Mediatech) plus 0.5 mg/ml collagenase type 1 (Worthington) and 2.5 mg/ml dispase protease type II (Cambrex) at 37°C for 4–6 hr. We plated trypan blue negative cells (STEMCELL) at 1 × 10^4 cells in 1 ml per well in 24-well low-binding plates in medium containing DMEM:F-12 (3:1) + 20 ng/ml rhEGF (R&D Systems), 20 ng/ml rh bFGF (R&D Systems), 1% B-27 (Invitrogen), and 2 μg/ml heparin (Sigma-Aldrich). We maintained cultures at 37°C and 5% CO_2 and counted floating spheres after 4–7 days. To passage, we centrifuged sphere cultures, which were dissociated and plated at 1 × 10^4 cells/ml in fresh sphere medium as described (Williams et al., 2008). For each experiment, we show a representative of three independent experiments.

Immunohistochemistry

Tissue was embedded in paraffin, and 6-μm sections were cut and stained with either H&E or toluidine blue or were incubated overnight at 4°C with the following antibodies: anti-S100β (Dako), Ki67 (Novacastra Leica Microsystems), anti-P-Stat3 (Y705), anti-cleaved caspase 3, or β-catenin (Cell Signaling Technology). Visualization methods were as described (Williams et al., 2008).

Western Blots

Western blots were performed using antibodies recognizing P-Jak2, Jak2, P-Stat3, Stat3, P-β-catenin, β-catenin, P-GSK3β, GSK3β, and β-actin (Cell Signaling Technology). At least three different tumor and/or cell lysates were analyzed per antigen.

Tumorigenesis Assay in Nude Mice

We injected 5 × 10^5 mouse sphere cells/injection subcutaneously into athymic female nude mice (Harlan). After 2 months we dissected tumors and fixed them in 4% paraformaldehyde overnight, which were then embedded in paraffin for histology.

Measurement of Tumor Number and Tumor Size

We perfused each mouse intracardially with 4% paraformaldehyde (w/v) in PBS, which were then incubated overnight in 300 ml 4% paraformaldehyde, incubated overnight, again, in 50 ml decalcification solution (Cal-Rite, Richard Allan Scientific), and then transferred to PBS. Using a Leica dissecting microscope, we dissected the spinal cord with attached DRG and nerve roots, and counted tumors. A tumor was defined as a mass surrounding the DRG and/or nerve roots, with a diameter greater than 1 mm, measured perpendicular to DRG and/or nerve roots.

Tumor Volumetric Measurement

MRI imaging and volumetric measurement of neurofibromas and statistical analyses using mixed effects modeling were as described (Wu et al., 2012).

Lentiviral Infection

We infected secondary *Nf1*$^{fl/fl}$*;DhhCre* neurofibroma spheres or *Stat3*$^{fl/fl}$*;Nf1*$^{fl/fl}$*;DhhCre* DRG/neurofibroma spheres with shRNA and non-target control (Sigma-Aldrich), β-catenin overexpression lentivirus ΔN90 (Addgene), or same backbone control (Sigma-Aldrich). We incubated lentiviral particles with neurofibroma spheres for 3–5 days and counted sphere numbers. For in vivo xenografts, *Stat3*$^{fl/fl}$*;Nf1*$^{fl/fl}$*;DhhCre* DRG/neurofibroma spheres were infected with lentivirus in the presence of polybrene (8μg/ml; Sigma-Aldrich) for 16–20 hr, followed by selection in G418 (500 mg/ml; Sigma-Aldrich). Spheres were collected and dissociated for xenograft injection.

Statistics

Kaplan-Meier analysis used a Gehan-Breslow-Wilcox log-rank test. Neurofibroma growth was modeled by mixed effects model analysis. p values were generated with a random effects model analysis of log transformed tumor volume data using the SAS mixed procedure (Jessen et al., 2013). We used unpaired two-tailed Student's t tests to analyze significance of cell proliferation and cell death quantification in tissue sections when two samples were compared. Other experiments used ordinary one-way ANOVA, reported as mean ± SEM; $p < 0.05$ was considered significant.

SUPPLEMENTAL INFORMATION

Supplemental Information includes Supplemental Experimental Procedures and seven figures and can be found with this article online at http://dx.doi.org/10.1016/j.celrep.2016.01.074.

AUTHOR CONTRIBUTIONS

Conceptualization and Methodology, N.R. and D.A.L.; Investigation, J.W., V.W.K., D.M.P., J.K.K., A.V.P., E.J., W.J.J., K.C., B.R.T., K.A.T.S., D.F., E.D., G.H., J.A.C., and A.O.S.-R.; Resources, E.B.S. and J.R.F (FLLL32), D.E.L. (*Stat3*$^{fl/fl}$ mouse), and R.J.S. (human samples); Formal Analysis, J.W., V.W.K., Y.Z., M.-O.K., N.R., and D.A.L.; Writing – Review and Editing, J.W., V.W.K., N.R., and D.A.L.

ACKNOWLEDGMENTS

We thank the Minnesota Supercomputing Institute for computational resources for sequence analysis, Dr. Ari Melnick (Weil Cornell Medical School) for assistance in design of histone modification analysis, and Ms. Huiqing Li for animal husbandry. This work was supported by NIH R01 NS28840 (N.R.), NIH P50 NS057531 (N.R. and D.A.L.), a DAMD New Investigator Award (W81XWH-11-1-0259), an Ohio State University Comprehensive Cancer Center Pelotonia Idea Grant (J.W.), and the American Cancer Society (IRG-67-003-44) (J.R.F.). The CHTN provided some benign neurofibromas used in this study.

Received: November 10, 2015
Revised: January 12, 2016
Accepted: January 23, 2016
Published: February 18, 2016

REFERENCES

Banerjee, S., Byrd, J.N., Gianino, S.M., Harpstrite, S.E., Rodriguez, F.J., Tuskan, R.G., Reilly, K.M., Piwnica-Worms, D.R., and Gutmann, D.H. (2010). The neurofibromatosis type 1 tumor suppressor controls cell growth by regulating signal transducer and activator of transcription-3 activity in vitro and in vivo. Cancer Res. *70*, 1356–1366.

Barker, N., Hurlstone, A., Musisi, H., Miles, A., Bienz, M., and Clevers, H. (2001). The chromatin remodelling factor Brg-1 interacts with beta-catenin to promote target gene activation. EMBO J. *20*, 4935–4943.

Battle, T.E., and Frank, D.A. (2002). The role of STATs in apoptosis. Curr. Mol. Med. *2*, 381–392.

Boyd, K.P., Korf, B.R., and Theos, A. (2009). Neurofibromatosis type 1. J. Am. Acad. Dermatol. *61*, 1–14, quiz 15–16.

Chen, Z., Liu, C., Patel, A.J., Liao, C.P., Wang, Y., and Le, L.Q. (2014). Cells of origin in the embryonic nerve roots for NF1-associated plexiform neurofibroma. Cancer Cell *26*, 695–706.

Cichowski, K., and Jacks, T. (2001). NF1 tumor suppressor gene function: narrowing the GAP. Cell *104*, 593–604.

De Raedt, T., Beert, E., Pasmant, E., Luscan, A., Brems, H., Ortonne, N., Helin, K., Hornick, J.L., Mautner, V., Kehrer-Sawatzki, H., et al. (2014). PRC2 loss amplifies Ras-driven transcription and confers sensitivity to BRD4-based therapies. Nature *514*, 247–251.

Faghihi, M.A., and Wahlestedt, C. (2009). Regulatory roles of natural antisense transcripts. Nat. Rev. Mol. Cell Biol. *10*, 637–643.

Grigoryan, T., Stein, S., Qi, J., Wende, H., Garratt, A.N., Nave, K.A., Birchmeier, C., and Birchmeier, W. (2013). Wnt/Rspondin/β-catenin signals control axonal sorting and lineage progression in Schwann cell development. Proc. Natl. Acad. Sci. USA *110*, 18174–18179.

Helming, K.C., Wang, X., Wilson, B.G., Vazquez, F., Haswell, J.R., Manchester, H.E., Kim, Y., Kryukov, G.V., Ghandi, M., Aguirre, A.J., et al. (2014). ARID1B is a specific vulnerability in ARID1A-mutant cancers. Nat. Med. *20*, 251–254.

Jessen, W.J., Miller, S.J., Jousma, E., Wu, J., Rizvi, T.A., Brundage, M.E., Eaves, D., Widemann, B., Kim, M.O., Dombi, E., et al. (2013). MEK inhibition exhibits efficacy in human and mouse neurofibromatosis tumors. J. Clin. Invest. *123*, 340–347.

Keng, V.W., Villanueva, A., Chiang, D.Y., Dupuy, A.J., Ryan, B.J., Matise, I., Silverstein, K.A., Sarver, A., Starr, T.K., Akagi, K., et al. (2009). A conditional transposon-based insertional mutagenesis screen for genes associated with mouse hepatocellular carcinoma. Nat. Biotechnol. *27*, 264–274.

Khursheed, M., Kolla, J.N., Kotapalli, V., Gupta, N., Gowrishankar, S., Uppin, S.G., Sastry, R.A., Koganti, S., Sundaram, C., Pollack, J.R., and Bashyam, M.D. (2013). ARID1B, a member of the human SWI/SNF chromatin remodeling complex, exhibits tumour-suppressor activities in pancreatic cancer cell lines. Br. J. Cancer *108*, 2056–2062.

Kim, D.J., Kataoka, K., Rao, D., Kiguchi, K., Cotsarelis, G., and Digiovanni, J. (2009). Targeted disruption of stat3 reveals a major role for follicular stem cells in skin tumor initiation. Cancer Res. *69*, 7587–7594.

Kroon, P., Berry, P.A., Stower, M.J., Rodrigues, G., Mann, V.M., Simms, M., Bhasin, D., Chettiar, S., Li, C., Li, P.K., et al. (2013). JAK-STAT blockade inhibits tumor initiation and clonogenic recovery of prostate cancer stem-like cells. Cancer Res. *73*, 5288–5298.

Lee, W., Teckie, S., Wiesner, T., Ran, L., Prieto Granada, C.N., Lin, M., Zhu, S., Cao, Z., Liang, Y., Sboner, A., et al. (2014). PRC2 is recurrently inactivated through EED or SUZ12 loss in malignant peripheral nerve sheath tumors. Nat. Genet. *46*, 1227–1232.

Lesina, M., Kurkowski, M.U., Ludes, K., Rose-John, S., Treiber, M., Klöppel, G., Yoshimura, A., Reindl, W., Sipos, B., Akira, S., et al. (2011). Stat3/Socs3 activation by IL-6 transsignaling promotes progression of pancreatic intraepithelial neoplasia and development of pancreatic cancer. Cancer Cell *19*, 456–469.

Lin, L., Hutzen, B., Zuo, M., Ball, S., Deangelis, S., Foust, E., Pandit, B., Ihnat, M.A., Shenoy, S.S., Kulp, S., et al. (2010). Novel STAT3 phosphorylation inhibitors exhibit potent growth-suppressive activity in pancreatic and breast cancer cells. Cancer Res. *70*, 2445–2454.

Liu, C., Li, Y., Semenov, M., Han, C., Baeg, G.H., Tan, Y., Zhang, Z., Lin, X., and He, X. (2002). Control of beta-catenin phosphorylation/degradation by a dual-kinase mechanism. Cell *108*, 837–847.

Luscan, A., Shackleford, G., Masliah-Planchon, J., Laurendeau, I., Ortonne, N., Varin, J., Lallemand, F., Leroy, K., Dumaine, V., Hivelin, M., et al. (2014). The activation of the WNT signaling pathway is a Hallmark in neurofibromatosis type 1 tumorigenesis. Clin. Cancer Res. *20*, 358–371.

Magistri, M., Faghihi, M.A., St Laurent, G., 3rd, and Wahlestedt, C. (2012). Regulation of chromatin structure by long noncoding RNAs: focus on natural antisense transcripts. Trends Genet. *28*, 389–396.

Mo, W., Chen, J., Patel, A., Zhang, L., Chau, V., Li, Y., Cho, W., Lim, K., Xu, J., Lazar, A.J., et al. (2013). CXCR4/CXCL12 mediate autocrine cell- cycle progression in NF1-associated malignant peripheral nerve sheath tumors. Cell *152*, 1077–1090.

Moh, A., Zhang, W., Yu, S., Wang, J., Xu, X., Li, J., and Fu, X.Y. (2008). STAT3 sensitizes insulin signaling by negatively regulating glycogen synthase kinase-3 beta. Diabetes *57*, 1227–1235.

Nagl, N.G., Jr., Wang, X., Patsialou, A., Van Scoy, M., and Moran, E. (2007). Distinct mammalian SWI/SNF chromatin remodeling complexes with opposing roles in cell-cycle control. EMBO J. *26*, 752–763.

Nakamura, T., Colbert, M.C., and Robbins, J. (2006). Neural crest cells retain multipotential characteristics in the developing valves and label the cardiac conduction system. Circ. Res. *98*, 1547–1554.

Ni, Z., and Bremner, R. (2007). Brahma-related gene 1-dependent STAT3 recruitment at IL-6-inducible genes. J. Immunol. *178*, 345–351.

Rahrmann, E.P., Watson, A.L., Keng, V.W., Choi, K., Moriarity, B.S., Beckmann, D.A., Wolf, N.K., Sarver, A., Collins, M.H., Moertel, C.L., et al. (2013). Forward genetic screen for malignant peripheral nerve sheath tumor formation identifies new genes and pathways driving tumorigenesis. Nat. Genet. *45*, 756–766.

Sausen, M., Leary, R.J., Jones, S., Wu, J., Reynolds, C.P., Liu, X., Blackford, A., Parmigiani, G., Diaz, L.A., Jr., Papadopoulos, N., et al. (2013). Integrated genomic analyses identify ARID1A and ARID1B alterations in the childhood cancer neuroblastoma. Nat. Genet. *45*, 12–17.

Serra, E., Puig, S., Otero, D., Gaona, A., Kruyer, H., Ars, E., Estivill, X., and Lázaro, C. (1997). Confirmation of a double-hit model for the NF1 gene in benign neurofibromas. Am. J. Hum. Genet. *61*, 512–519.

Sherry, M.M., Reeves, A., Wu, J.K., and Cochran, B.H. (2009). STAT3 is required for proliferation and maintenance of multipotency in glioblastoma stem cells. Stem Cells *27*, 2383–2392.

Tolstorukov, M.Y., Sansam, C.G., Lu, P., Koellhoffer, E.C., Helming, K.C., Alver, B.H., Tillman, E.J., Evans, J.A., Wilson, B.G., Park, P.J., and Roberts, C.W. (2013). Swi/Snf chromatin remodeling/tumor suppressor complex establishes nucleosome occupancy at target promoters. Proc. Natl. Acad. Sci. USA *110*, 10165–10170.

Trotter, K.W., and Archer, T.K. (2008). The BRG1 transcriptional coregulator. Nucl. Recept. Signal. *6*, e004.

Vasileiou, G., Ekici, A.B., Uebe, S., Zweier, C., Hoyer, J., Engels, H., Behrens, J., Reis, A., and Hadjihannas, M.V. (2015). Chromatin-Remodeling-Factor ARID1B Represses Wnt/β-Catenin Signaling. Am. J. Hum. Genet. *97*, 445–456.

Watson, A.L., Rahrmann, E.P., Moriarity, B.S., Choi, K., Conboy, C.B., Greeley, A.D., Halfond, A.L., Anderson, L.K., Wahl, B.R., Keng, V.W., et al. (2013). Canonical Wnt/β-catenin signaling drives human schwann cell transformation, progression, and tumor maintenance. Cancer Discov. *3*, 674–689.

Williams, J.P., Wu, J., Johansson, G., Rizvi, T.A., Miller, S.C., Geiger, H., Malik, P., Li, W., Mukouyama, Y.S., Cancelas, J.A., and Ratner, N. (2008). Nf1 mutation expands an EGFR-dependent peripheral nerve progenitor that confers neurofibroma tumorigenic potential. Cell Stem Cell *3*, 658–669.

Wu, D., and Pan, W. (2010). GSK3: a multifaceted kinase in Wnt signaling. Trends Biochem. Sci. *35*, 161–168.

Wu, J., Williams, J.P., Rizvi, T.A., Kordich, J.J., Witte, D., Meijer, D., Stemmer-Rachamimov, A.O., Cancelas, J.A., and Ratner, N. (2008). Plexiform and dermal neurofibromas and pigmentation are caused by Nf1 loss in desert hedgehog-expressing cells. Cancer Cell *13*, 105–116.

Wu, J., Dombi, E., Jousma, E., Scott Dunn, R., Lindquist, D., Schnell, B.M., Kim, M.O., Kim, A., Widemann, B.C., Cripe, T.P., and Ratner, N. (2012). Preclincial testing of sorafenib and RAD001 in the Nf(flox/flox); DhhCre mouse model of plexiform neurofibroma using magnetic resonance imaging. Pediatr. Blood Cancer *58*, 173–180.

Wu, J., Patmore, D.M., Jousma, E., Eaves, D.W., Breving, K., Patel, A.V., Schwartz, E.B., Fuchs, J.R., Cripe, T.P., Stemmer-Rachamimov, A.O., and Ratner, N. (2014). EGFR-STAT3 signaling promotes formation of malignant peripheral nerve sheath tumors. Oncogene *33*, 173–180.

Zhu, Y., Ghosh, P., Charnay, P., Burns, D.K., and Parada, L.F. (2002). Neurofibromas in NF1: Schwann cell origin and role of tumor environment. Science *296*, 920–922.